C.E. SACLAY
DSM

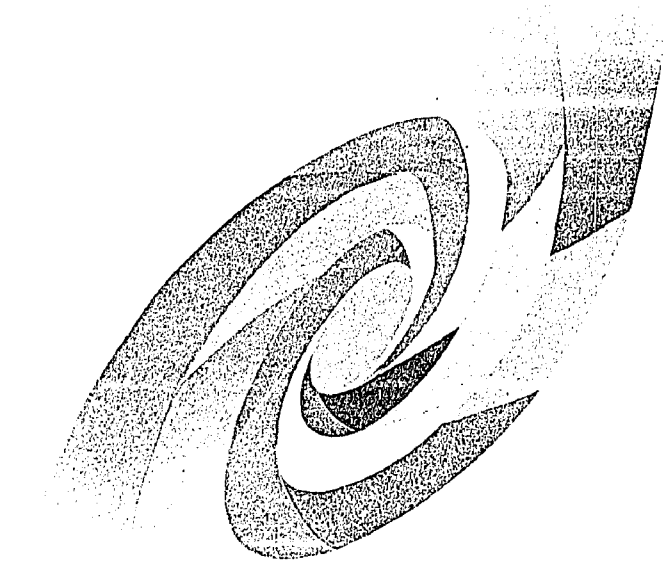

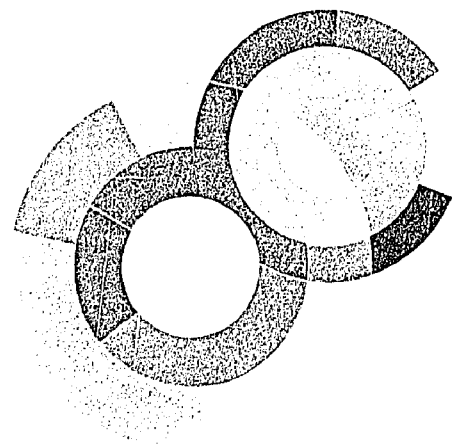

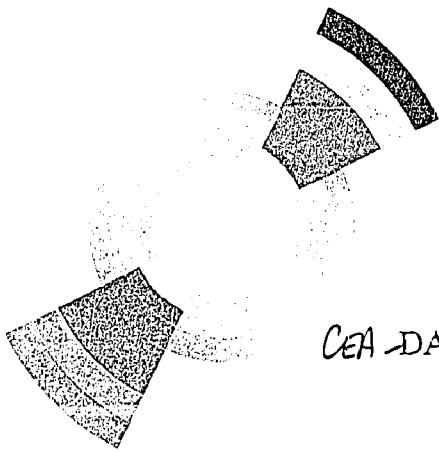

CEA-DAPNIA-SPhN-95-58 12/1995

NEUTRON PAIR AND PROTON PAIR TRANSFER REACTIONS BETWEEN IDENTICAL CORES IN THE SULFUR REGION

Michel C. Mermaz and Michel Girod

DAPNIA

VOL 27 № 17

Le DAPNIA (Département d'Astrophysique, de physique des Particules, de physique Nucléaire et de l'Instrumentation Associée) regroupe les activités du Service d'Astrophysique (SAp), du Département de Physique des Particules Elémentaires (DPhPE) et du Département de Physique Nucléaire (DPhN).

Adresse : DAPNIA, Bâtiment 141
CEA Saclay
F - 91191 Gif-sur-Yvette Cedex

Submitted to Phys. Rev. C

NEUTRON PAIR AND PROTON PAIR TRANSFER REACTIONS BETWEEN IDENTICAL CORES IN THE SULFUR REGION

Michel C. Mermaz

Commissariat à l'Energie Atomique,

Service de Physique Nucléaire, Centre d'études de Saclay

91191 Gif sur Yvette, Cedex, France

Michel Girod

Commissariat à l'Energie Atomique,

Service de Physique et Techniques Nucléaires,

Boîte Postale 12, 91680 Bruyères-le-Châtel, France

Abstract

Optical model and exact finite range distorted-wave Born approximation analyses were performed on neutron pair exchange between identical cores for ^{32}S and ^{34}S nuclei and on proton pair exchange between identical cores for ^{30}Si and ^{32}S. The extracted spectroscopic factors were compared with theoretical ones deduced from Hartree-Fock calculations on these pair of nuclei. The enhancement of the experimental cross sections with respect to the theoretical ones strongly suggests evidence for a nuclear Josephson effect.

21.10.Jx, 21.60Jz, 24.10.Ht and 24.50.+g

I. INTRODUCTION

With regard to angular distribution shape, two neutron transfer reactions between identical colliding cores have been successfully analyzed on the basis of phenomenological diffractional model [1] for the $^{32}S(^{34}S, ^{32}S)$ elastic scattering reaction measured at 97 MeV incident energy [2]. In this article, we present a standard optical model analysis and an exact finite range distorted wave Born approximation (EFR-DWBA) analysis of such reaction in order to investigate a possible nuclear Josephson effect for the neutron pair transfer reaction in the vicinity of the coulomb barrier [3]. Same analysis is also performed for the proton pair exchange between identical colliding cores of the $^{30}Si(^{32}S, ^{30}Si)$ reaction [2]. We define the nuclear Josephson effect in this paper as the simple enhancement of one identical nucleon pair transfer between cores due to the coherent nature of nuclear states in both nuclei exhibiting Bardeen-Cooper-Schrieffer (BCS) pair identical nucleon wavefunctions. During the collisions, a time dependent Josephson junction is formed between the two cores, the Coulomb barrier acting as an insulator. This was first pointed out by Gol'danskii and Larkin [4]. This nuclear Josephson effect can persist slightly above the Coulomb barrier [3].

The cross section for such an elastic scattering can be written

$$\sigma(\theta) = |f_{el.}(\theta) + \sqrt{NS_iS_f} f_{DWBA}(\pi - \theta)|^2. \quad (1)$$

For a zero spin system. Here $f_{el.}(\theta)$ is the usual elastic scattering amplitude given by an optical model analysis while $f_{DWBA}(\pi - \theta)$ is the direct EFR-DWBA transfer reaction amplitude. The values S_i and S_f are the entrance and exit channel spectroscopic factors and N a normalization factor equal to 1, if the direct surface transfer reaction model is perfectly suitable. If the incident energy is sufficiently above the coulomb barrier, the forward angle will be dominated by the elastic scattering while the backward angle cross section will be mainly the direct EFR-DWBA cross section.

II. SPECTROSCOPIC FACTOR

The spectroscopic amplitude A_{LSJ} for two nucleons coupled to S=0 or 1 is given for a 0s relative motion by [5]:

$$A_{LSJ} = g\sqrt{(2j_1+1)(2j_2+1)(2L+1)(2S+1)} \begin{Bmatrix} l_1 & 1/2 & j_1 \\ l_2 & 1/2 & j_2 \\ L & S & J \end{Bmatrix} < n_1, l_1, n_2, l_2 | N, l, 0, 0 > . \tag{2}$$

The value g is equal to 1, if the two nucleons are in the same subshell and otherwise equal to $\sqrt{2}$. The pair of accolades is the standard 9j Wigner symbol and the bracket $< \mid >$ is the Talmi-Moshinsky coefficient for a 0s relative motion and a N L center of mass motion. In our case, for a pair of identical nucleons, protons or neutrons, the total spin is equal to 0. Furthermore for 0^+ ground state configuration, we have: L=J=0 and $n_1 = n_2$, $l_1 = l_2$, $j_1 = j_2$.

In case of the wavefunction extend on several pure shell model configurations, the pick-up spectroscopic factor S_i is given by:

$$S_i = |\sum_{nk} V_{nk} A_{LSJ}(nlj)|^2, \tag{3}$$

where V_{nk} is the configuration amplitude and A_{LSJ} the corresponding spectroscopic amplitude while for stripping reaction, the spectroscopic factor S_f is given by:

$$S_f = |\sum_{nk} (1 - V_{nk}) A_{LSJ}(nlj)|^2, \tag{4}$$

with the same notation as previously. In the following section is presented the microscopic framework in which the configuration amplitudes V_{nk} are obtained.

III. SPECTROSCOPIC FACTORS FROM THE HARTREE-FOCK-BOGOLIUBOV THEORY AND CONFIGURATION MIXING CALCULATIONS

A. Theory

The theoretical framework within which are described the nuclear structure of ^{30}Si and ^{32,34}S is the generator coordinate method [6].

In the first step, potential energy surfaces (PESs) are built from constrained Hartree-Fock-Bogoliubov (HFB) calculations, i.e. from a minimization of the energy functional [7]

$$\delta < \Phi_q|\hat{H} - \lambda_0\hat{Q}_{20} - \lambda_2\hat{Q}_{22} - \lambda_Z\hat{Z} - \lambda_N\hat{N}|\Phi_q >= 0.$$

In this equation,

i) Φ_q is the quasiparticle (qp) vacuum,

ii) $\hat{H}$ is the many-body nuclear Hamiltonian $\hat{H} = \sum_{i=1}^{A} T_i + 1/2 \sum_{i \neq j} v_{ij}$, where T_i is the kinetic energy of the i^{th} nucleon, and v_{ij} the finite range density dependent force of Gogny [8],

iii) $\hat{Q}_{20}$ and $\hat{Q}_{22}$ are external field operators which generate axial and triaxial quadrupole deformations, respectively, and $\hat{Z}$ and $\hat{N}$ are the proton and neutron numbers, respectively.

Finally, the Lagrange multipliers λ_i are determined by the constraints $< \Phi_q|\hat{Q}_{2i}|\Phi_q >= q_{2i}$, and $< \Phi_q|\hat{Z}(or\hat{N})|\Phi_q >= Z(or N)$.

Once the constrained HFB equations are solved, the potential energy surface is defined as

$$V(q) =< \Phi_q|\hat{H}|\Phi_q >, \tag{5}$$

where the notation q = (q_{20}, q_{22}) is used. Since q_{20} and q_{22} are directly related to the Bohr coordinates β and γ, the potential energy surface (5) may also be expressed as V(β,γ).

In the second step, the dynamical states (i.e. the ground state and excited levels) are sought as

$$|\Psi >= \int f(q)|\Phi_q > dq,$$

where the superposition amplitude $f(q)$ is solution of the Griffin, Hill and Wheeler (GHW) equation [9]

$$\int [H(q,q') - EI(q,q')]f(q')dq' = 0. \tag{6}$$

In this equation, $H(q,q') =< \Phi_q|\hat{H}|\Phi_{q'} >$ is the nuclear kernel, $I(q,q') =< \Phi_q|\Phi_{q'} >$ the overlap kernel, and E the energy.

In the third (and final) step, it is assumed that $I(q,q')$ is a Gaussian shape. Under this so-called Gaussian overlap approximation [6], eq.(2) can be transformed into a second-order differential equation and expressed in the laboratory system

$$\hat{\mathcal{H}}g(q) = Eg(q),$$

where

$$\hat{\mathcal{H}} = -\frac{\hbar^2}{2}\sum_{i,j}\frac{\partial}{\partial q_i}(M^{-1}(q))_{ij}\frac{\partial}{\partial q_j} + \mathcal{V}(q) \tag{7}$$

is the collective Hamiltonian, $g(q)$ the Gauss transform of $f(q)$, and $\mathcal{V}(q)$ the potential energy surface corrected for zero-point energy $\Delta V(q)$ (i.e. $\mathcal{V}(q)$ = V(q) - $\Delta V(q)$). $\hat{\mathcal{H}}$ is formally identical to the Bohr Hamiltonian considered by Kumar and Baranger [10]:

$$\hat{\mathcal{H}} = \mathcal{V}(\beta_0,\beta_2) + \frac{1}{2}(B_{00}\dot{\beta}_0^2 + 2B_{02}\dot{\beta}_0\dot{\beta}_2 + B_{22}\dot{\beta}_2^2) + \sum_{k=1}^{3}\frac{< I_i^2 >}{2\mathcal{I}_i} \tag{8}$$

where the collective variables β_0, β_2 are related to the standard Bohr parameters by $\beta_0 = \beta\cos\gamma$, $\beta_2 = \beta\sin\gamma$, and to the quadrupole moments by $\sqrt{\frac{\pi}{5}}\frac{q_0}{r_0^2A^{5/3}}$ and $\sqrt{\frac{3\pi}{5}}\frac{q_2}{r_0^2A^{5/3}}$, respectively.

The zero-point energy term as well as the collective masses $B_{ij}(i,j = 0,2)$ and moments of inertia $\mathcal{I}_i(i = 1,3)$ which completely define the tensor M_{ij}, are calculated in the cranking approximation [11]. Let us note that the only ingredient used in our set of calculations is the Gogny force. With it, pairing correlations are handled in a fully microscopic way requiring no additional parameters [8]. The collective Hamiltonian $\hat{\mathcal{H}}$ is parameter free.

B. Spectroscopic factor

The lowest eigenvalue of this Hamiltonian is the correlated ground state (g.s.) energy. The higher ones are excitation energies of even parity rotational-vibrational collective levels. The corresponding eigenvectors, the collective wavefunctions, are used to calculate the g.s. observable quantities. The quantities we are interested here are the configuration amplitudes V_{nk}. In the HFB framework, these quantities are the occupation probabilities of particle states obtained from the constrained HFB calculations. In first approximation, we can considered that the nucleus is well described by the HFB wavefunction corresponding to the minimum of the PES. We give below the values of the V_{nk} obtained in this way, see table I. Next a better result may be deduced from mixing the constrained HFB solutions using the GHW formalism. Including these correlations in the g.s. wavefunction leads to significant changes in the predicting occupation probabilities which are defined in this framework as

$$V_{nk}^{dyn} = \int V_{nk}(\beta_0, \beta_2) g_{nk}(\beta_0, \beta_2)\ d\beta_0\ d\beta_2,$$

where $g_{nk}(\beta_0, \beta_2)$ is the g.s. collective wavefunction, (See figure 1).

IV. HFB RESULTS

A. Potential Energy Surfaces

The PES calculations are shown in figure 1. At first sight, these three PES's present very different structure. A prolate minimum at large deformation is seen for ^{32}S while an oblate minimum takes place at small deformation for ^{34}S. In contrast, no sharp minimum exists for ^{30}Si. For this last nucleus, it is clear that the wavefunction corresponding to the minimum of the PES will not be appropriate for the ground state. It is for this nucleus that the effect of the long range correlations are the most important.

B. Collective levels and transition probabilities

The collective level energies obtained for ^{30}Si and ^{32,34}S are shown in figure 2. Although here we are only interested in the ground state properties, the rather good agreement obtained for the first collective levels gives some confidence in our calculations. To further check the validity of our collective level predictions, we have calculated reduced transition probabilities for E2 transitions. In Table II is shown a comparison between measured [12] and predicted B(E2) values. The good agreement which is obtained suggests that our predictive collective wavefunctions are also reliable for the calculation of the V_{nk}'s.

In one hand, for the pick-up spectroscopic factors, it has turned out in the Hartree-Fock calculations for ^{34}S nucleus that the 1d5/2 and the 2s1/2 neutron shells are completely full while two pair of neutrons occupies the 1d3/2 shell. In the same vein for ^{30}Si nucleus, it appears that the 1d5/2 proton shell is also completely full. On the other hand for the stripping spectroscopic factors, it has turned out in the same calculations that the ground state wavefunction of ^{34}S is only the ground state wavefunction of ^{32}S coupled to a pair of neutrons in the 1d3/2 shell. In the same way, the ground state wavefunction of ^{32}S is only the ground state wavefunction of ^{30}Si coupled to a pair of protons in the 2s1/2 shell. Furthermore, it appears in all of these calculations that the 0f-1p shell is completely empty. Thus the neutron pair transfer as well as the proton pair transfer occur only on the 1s-0d shell orbitals and consequently the number of nodes of the center of mass motion is then equal to 2.

V. THE OPTICAL MODEL AND EFR-DWBA ANALYSIS

Figures 3 and 4 present an optical model analysis and EFR-DWBA analysis of the complete elastic scattering plus transfer angular distributions of ^{32}S(^{34}S, ^{32}S) reaction obtained with the code SATURN-MARS [13]. The optical model elastic scattering parameters which best fit the data at forward angles (angles smaller than 80 deg. c.m.) are given in table

III, families V1 and V2 and where obtained with the automatic search code PTOLEMY [14]. These parameters correspond to strong absorption using equal geometry for real and imaginary part of a Saxon-Woods potential. The phase of the wiggles at backward angles are perfectly reproduced. The agreement is strikingly good at 97 MeV ^{32}S incident energy. The extracted experimental value NS_iS_f spectroscopic factor which best fit the data points is 1.70 for a theoretical Hartree-Fock value of S_iS_f= 0.13. The experimental enhancement factor N is then about 13. In case of transfer reactions between identical core, we have in the same figure the agreement between elastic scattering fit at forward angles and quasi elastic transfer reaction cross section at backward angles leaving no freedom for the adjustment of the optical model parameters. The bound states well parameters are the reduced radius r=1.25 fm and the diffusivity a=0.65 fm. The reduced radius r is already large and favors quite a bit the transfer reaction. The bound state wavefunctions according the Talmi-Moshinsky transformation have two nodes. At very backward angles, the experimental points are well above the theoretical fit and correspond to a region of distant collision where the transfer reaction can occur only through Josephson tunneling of Cooper pair.

Figure 5 presents the very same analysis for proton pair transfer reaction between identical cores of the $^{30}Si(^{32}S, ^{30}Si)$. The optical model parameters which best fit the data points are given in table III, family V3 and correspond to strong absorption potential. The deviation had very backward angle between the experimental points and the fit can be due to a possible Josephson effect as already pointed out in the neutron pair transfer reaction case. The extracted experimental value NS_iS_f spectroscopic factor is 3.0 for a theoretical Hartree-Fock value of S_iS_f= 0.23. We have now an experimental enhancement factor of almost 13.

VI. DISCUSSION AND CONCLUSION

The unhappiness factor N is too high by factor 13 for the ^{34}S, ^{32}S reaction and too high also by a factor 13 for the ^{30}Si, ^{32}S reaction which means for both system that the pair trans-

fer reactions are much too large at backward angles. Let us note, that the spectroscopic factors are the largest values which can be obtained for a classical transfer reaction process. The optical model parameters reproduce extremely well the elastic angular distributions at forward angles and also the interference pattern between elastic scattering and transfer process, in the intermediate angular range for both reactions. This means that the pure transfer reaction is correctly computed and that the deviation from the theoretical absolute values and the disagreement in shape observed at very backward angles can be due to a possible Josephson effect: current of Cooper pair between the two colliding cores. This tunnelling current of pair has to be high at very backward angles where a distant collision occurs due to the Coulomb plus centrifugal barrier playing the role of insulator layer between the two super-conducting fluid. Nevertheless, there is a caveat to this last statement: unhappiness factor can be larger than one in pair transfer reactions as observed by the authors of reference [15] where a factor 2.3 is encountered for N, in the ^{74}Ge(^{18}O, ^{16}O)^{76}Ge and ^{76}Ge(^{16}O, ^{18}O)^{74}Ge reactions due to the possible neglect of sequential processes.

ACKNOWLEDGMENTS

Sincere thanks are due to Professor B. BILWES of the University of Louis Pasteur, Strasbourg for having provided us with her beautiful data on scattering of ^{32}S beam on ^{28}Si and on ^{34}S target nuclei, in tabulated form.

REFERENCES

[1] M.C. Mermaz, B. Bilwes, R. Bilwes and J.L. Ferrero, Phys. Rev. C27, 2408, (1983).

[2] J.L. Ferrero, J.A. Ruiz, B. Bilwes and R. Bilwes, Nucl. Phys. A510 , 360 (1990).

[3] K. Dietrich, Phys. Lett. **32B**, 428 (1970), Ann. Phys. (N.Y.)66, 480 (1971); K. Dietrich, in Brazilian Symposium on Theoretical Physics, edited by E. Ferreira (*Livros Tecnicos e Cientificos, Rio de Janeiro, 1975*) Vol. 2 p. 213; H. Weiss, Phys. Rev. C19, 834 (1979).

[4] V.I. Gol'danskii and A.I. Larkin, Zh Eksp. Theor. Fiz **53**, 1032 (1967) [Sov. Phys.—JETP **26**, 617 (1968)].

[5] P. Bonche, private communication.

[6] P. Ring and P. Schuck, The Nuclear Many-Body Problem (Springer, Berlin, 1980), p. 398.

[7] M. Girod and B. Grammaticos, Phys. Rev. **C27**, 2317 (1983).

[8] J. Dechargé and D. Gogny, Phys. Rev. C21, 1568 (1980); J. F. Berger, M. Girod, and D. Gogny, Nucl. Phys. A428, 23c (1984); ibid. A502, 85c (1989); ibid. Comp. Phys. Comm. 63, 365 (1991).

[9] D. L. Hill and J. A. Wheeler, Phys. Rev. 89, 1102 (1953); J. J. Griffin and J. A. Wheeler, Phys. Rev. 108, 311 (1957).

[10] K. Kumar and M. Baranger, Nucl. Phys. A110, 529 (1968); K. Kumar, B. Remaud, P. Auger, J. S. Vaagen, A. C. Rester, R. Foucher, and J. H. Hamilton, Phys. Rev. C16, 1235 (1977).

[11] B. Giraud, and B. Grammaticos, Nucl. Phys. A233, 373 (1974); ibid. A255, 141 (1975); M. Girod and B. Grammaticos, Nucl. Phys. A330, 40 (1979) and references therein.

[12] S. Raman C.H. Malarkey, W.T. Milner, C.W. Nestor, Jr. and P.H. Stelson, Atomic Data and Nuclear Data Tables 36, 19 (1987)

[13] Saclay modified version, T. Tamura and K.S. Low, Computer Phys. communications 8, 349 (1974).

[14] M.H. Macfarlane and S.C. Pieper, Argonne National Laboratory Report ANL 76-11 Rev.1, Mathematics and computers UC-32, (1976)

[15] M.-C. Lemaire and K.S. Low, Phys. Rev. C16, 183, (1977).

FIGURES

FIG. 1. The potential energy surface for ^{30}Si and ^{32,34}S nuclei on the left part, and on the right part, the corresponding ground state collective wavefunctions.

FIG. 2. Experimental and theoretical level scheme of the ^{30}Si and ^{32,34}S nuclei for the first even collective states

FIG. 3. Angular distribution of the ^{32}S(^{34}S, ^{32}S) elastic scattering plus transfer reaction between identical cores measured at 90 MeV ^{32}S incident energy. The experimental data points are from the work of J.L. Ferrero *et al.*

FIG. 4. Angular distribution of the ^{32}S(^{34}S, ^{32}S) elastic scattering plus transfer reaction between identical cores measured at 97 MeV ^{32}S incident energy. The experimental data points are from the work of J.L. Ferrero *et al.*

FIG. 5. Angular distribution of the ^{30}Si(^{32}S, ^{30}Si) elastic scattering plus transfer reaction between identical cores measured at 90 MeV ^{32}S incident energy. The experimental data points are from the work of J.L. Ferrero *et al.*

TABLES

	^{30}Si(p)		^{32}S(p)		^{32}S(n)		^{34}S(n)	
	$V_{nk}^{2\,dyn}$	V_{nk}^2	$V_{nk}^{2\,dyn}$	V_{nk}^2	$V_{nk}^{2\,dyn}$	V_{nk}^2	$V_{nk}^{2\,dyn}$	V_{nk}^2
1d5/2-1/2	0.996	1.00	0.998	1.00	0.997	1.00	0.996	1.00
1d5/2-3/2	0.990	1.00	0.997	1.00	0.995	1.00	0.995	1.00
1d5/2-5/2	0.891	1.00	0.992	1.00	0.987	1.00	0.990	1.00
2s1/2-1/2	0.111	0.6E-04	0.914	1.00	0.883	1.00	0.974	1.00
1d3/2-1/2	0.006	0.5E-04	0.081	0.7E-04	0.099	0.5E-04	0.783	0.999
1d3/2-3/2	0.002	0.4E-05	0.003	0.2E-04	0.008	0.2E-04	0.167	0.7E-03

TABLE I. Theoretical occupation probabilities V_{nk}^2 for ^{30}Si, ^{32}S, and ^{34}S nuclei. For each nucleus, the first column corresponds to $V_{nk}^{2\,dyn}$ and the second one to V_{nk}^2 at the minimum of the PES

Nucleus	B(E2)↑ Exp.[a]	B(E2)↑ Theo.
^{30}Si	0.0215	0.0252
^{32}S	0.0300	0.0307
^{34}S	0.0212	0.0258

TABLE II. Experimental and theoretical transition probabilities B(E2) in e^2b for ^{32}S, ^{34}S and ^{30}Si nuclei.[a] from the compilation of S.Raman *et al.*

Target	^{34}S	^{34}S	^{30}Si
$E_{Lab.}(MeV)$	90.0	97.0	90.0
Potential family	V1	V2	V3
$V(MeV)$	50.0	50.0	50.0
$W(MeV)$	20.0	20.0	20.0
$r_0(fm)$	1.274	1.285	1.288
$a_0(fm)$	0.517	0.495	0.494

TABLE III. Optical model parameter table for ^{32}S projectile on ^{34}S and ^{30}Si target nuclei. The geometry are the same for the real and the imaginary part. The reduced Coulomb radius r_c is equal to the real part optical model radius r_0 .

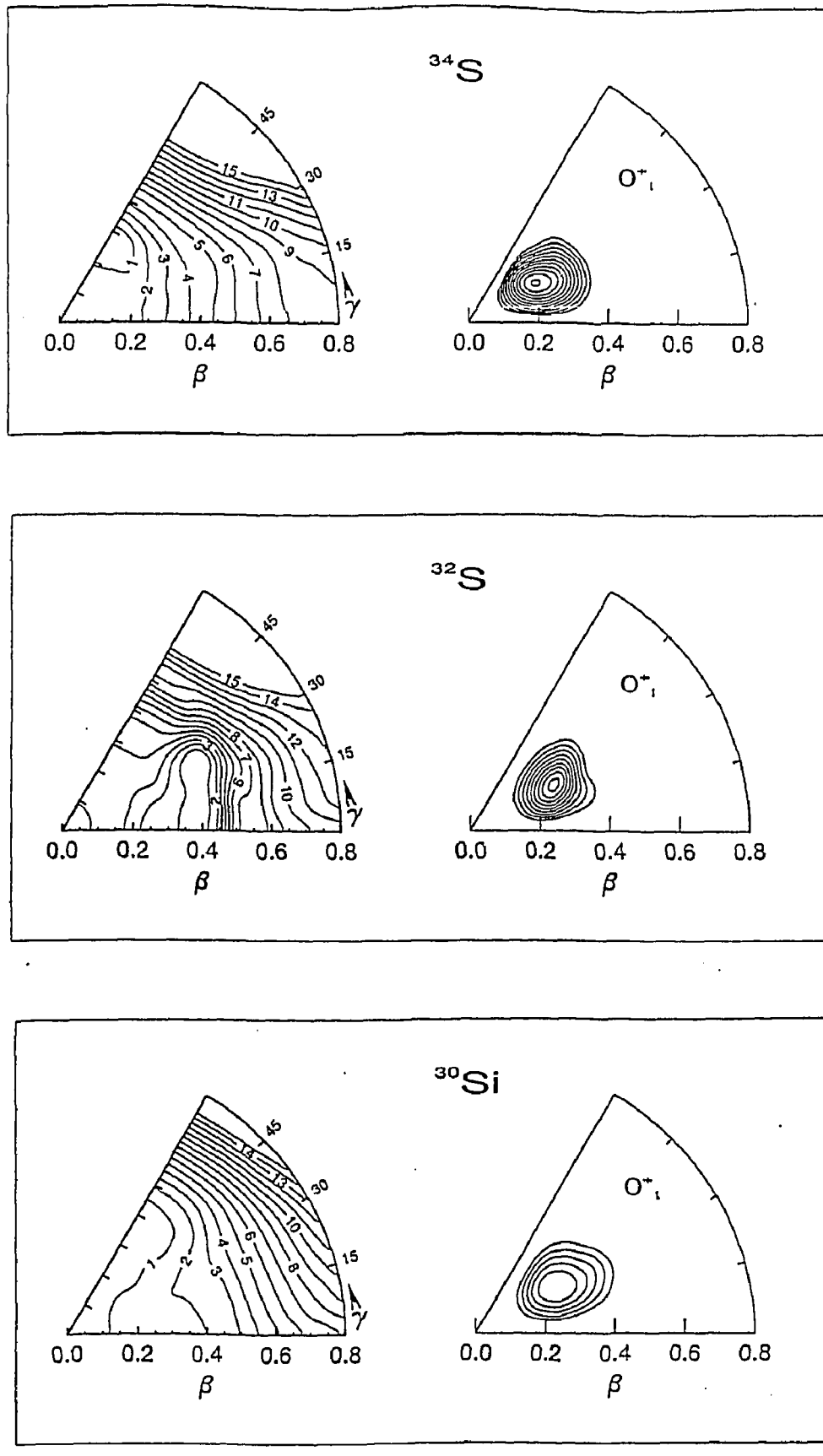

Fig. 1

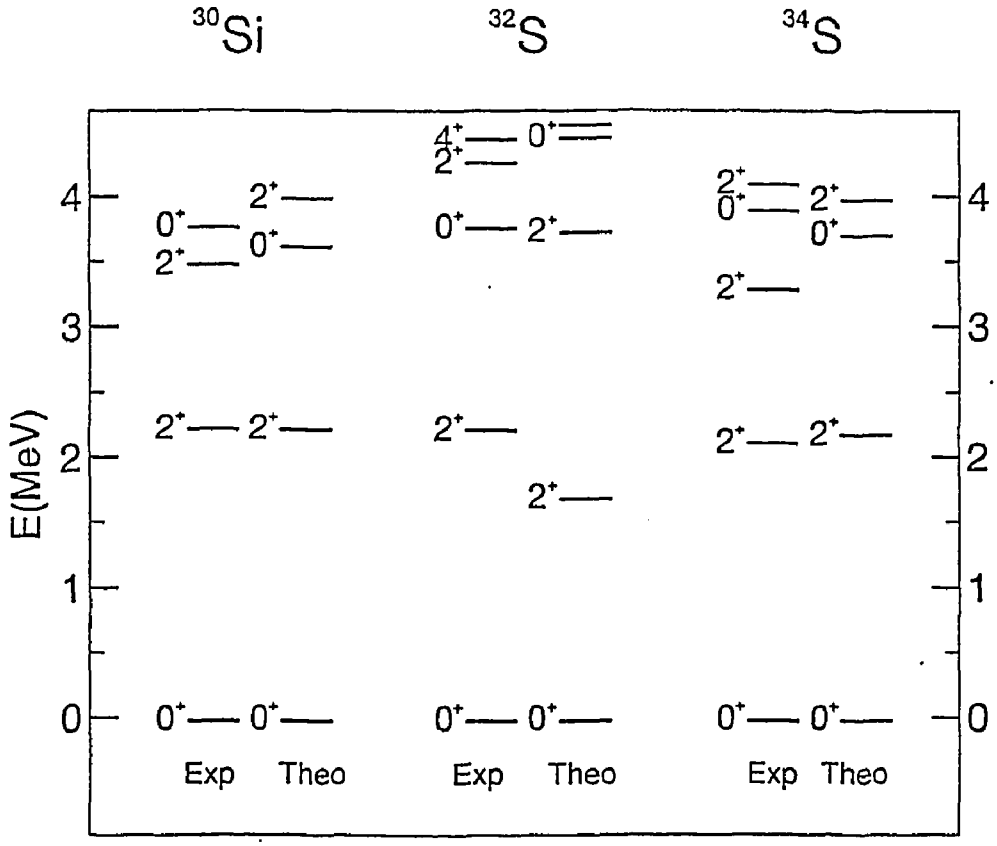

Fig. 2

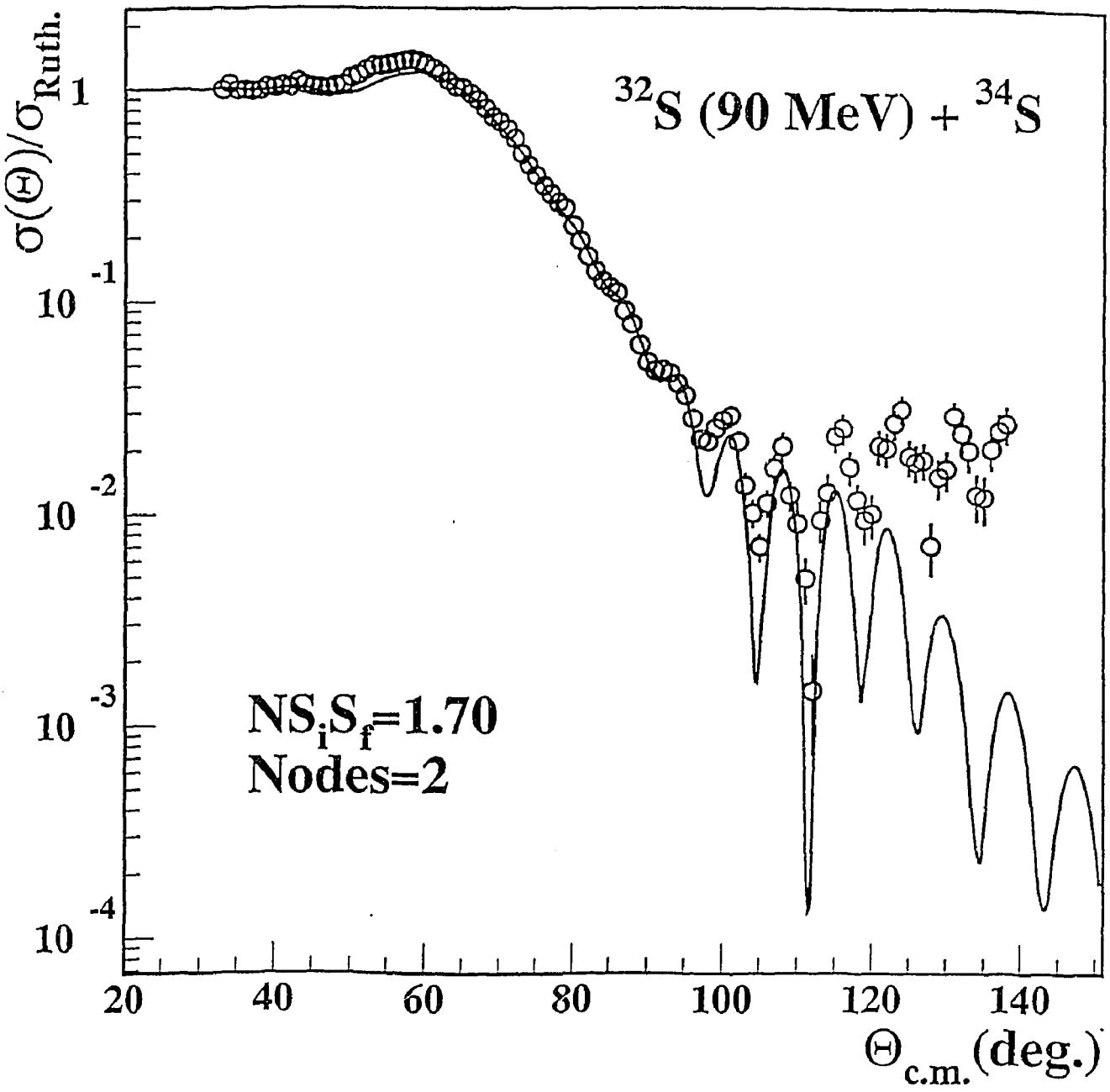
$\sigma(\Theta)/\sigma_{Ruth.}$
1
10^{-1}
10^{-2}
10^{-3}
10^{-4}
^{32}S (90 MeV) + ^{34}S
NS_iS_f=1.70
Nodes=2
20
40
60
80
100
120
140
$\Theta_{c.m.}$(deg.)

Fig. 3

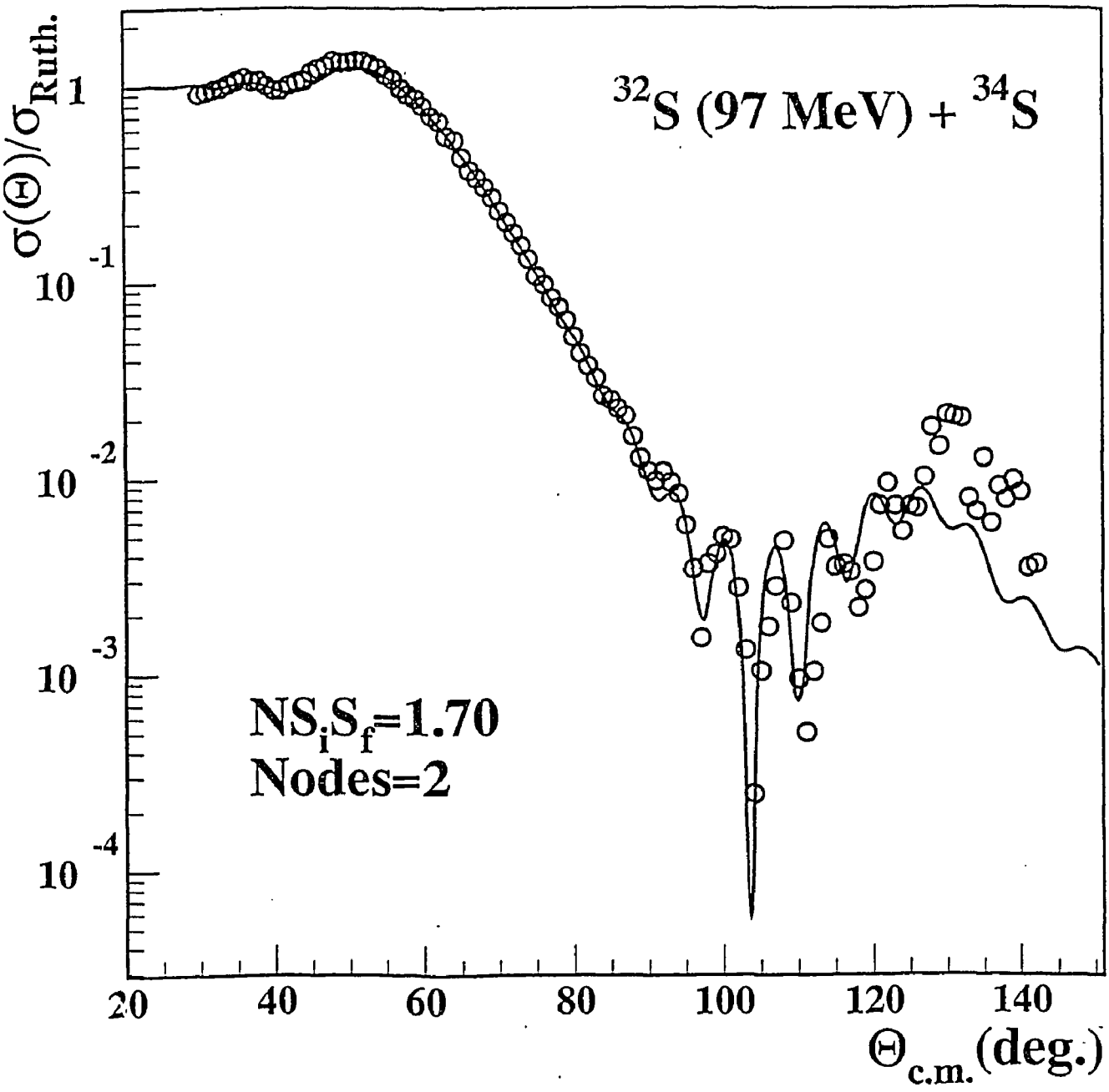
^{32}S (97 MeV) + ^{34}S
NS_iS_f=1.70
Nodes=2
$\sigma(\Theta)/\sigma_{Ruth.}$
1
10^{-1}
10^{-2}
10^{-3}
10^{-4}
20
40
60
80
100
120
140
$\Theta_{c.m.}$(deg.)

Fig. 4

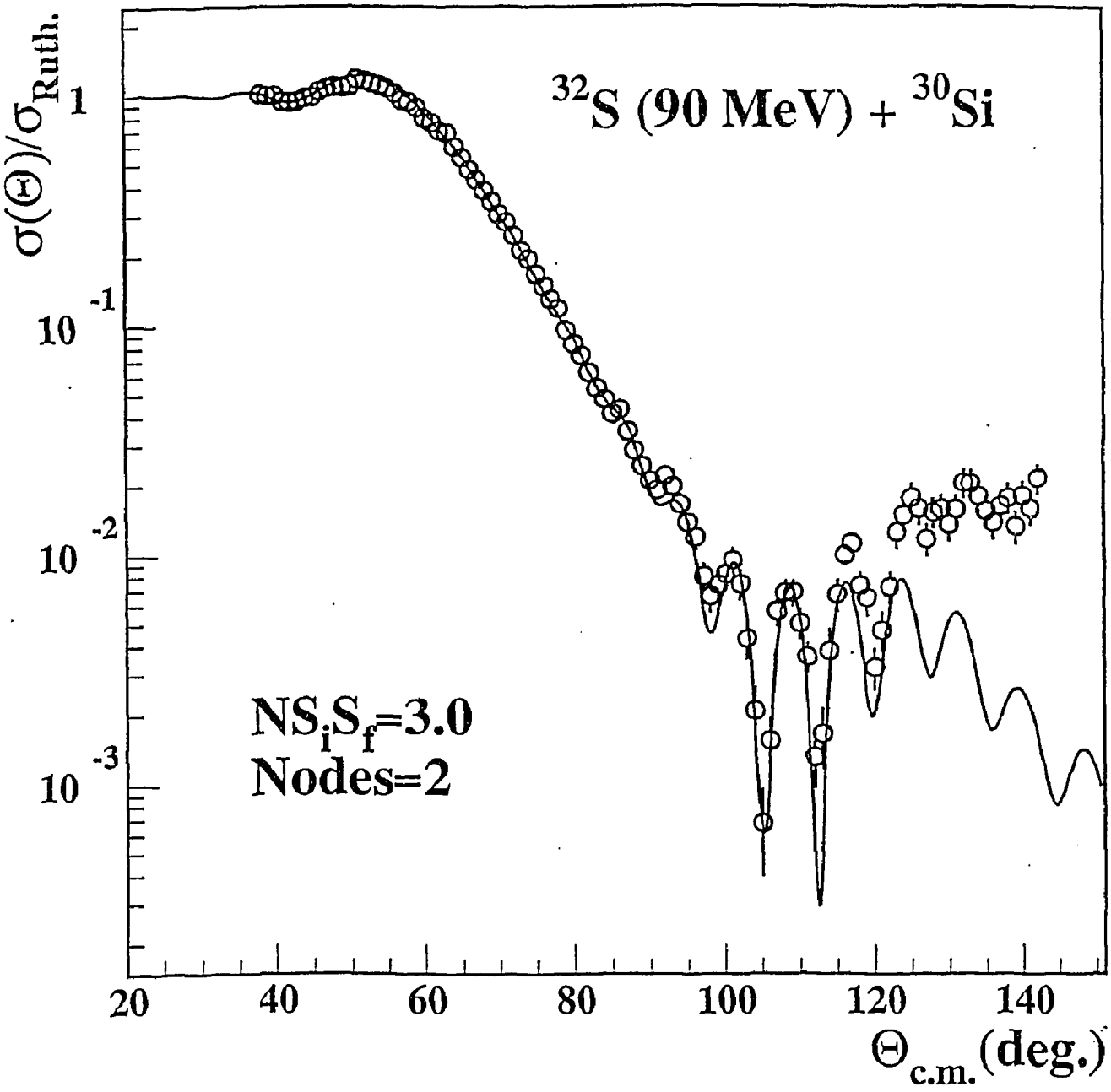
^{32}S (90 MeV) + ^{30}Si
NS_iS_f=3.0
Nodes=2
$\sigma(\Theta)/\sigma_{Ruth.}$
1
10^{-1}
10^{-2}
10^{-3}
20
40
60
80
100
120
140
$\Theta_{c.m.}$(deg.)

Fig. 5